Available online at www.sciencedirect.com

SciVerse ScienceDirect

Procedia Engineering 00 (2015) 000–000

Procedia Engineering

www.elsevier.com/locate/procedia

XXIII Italian Group of Fracture Meeting, IGFXXIII

Analytical modelling of the pullout behavior of synthetic fibres treated with nano-silica

Enrico Radi[a,*], Luca Lanzoni[b], Andrea Sorzia[a]

[a]*Dipartimento di Scienze e Metodi dell'Ingegneria, Via Amendola 2, Reggio Emilia 42122, ITALY*
[b]*Dipartimento di Ingegneria "Enzo Ferrari", Via Pietro Vivarelli 10, Modena 41125, ITALY*

Abstract

An accurate one-dimensional analytical model for simulating the pullout process of synthetic fibres from a cement matrix is proposed in the present study in order to shed light on the ductile behavior exhibited by Fibre Reinforced Concrete (FRC) members. The proposed model is able to predict the non linear relation between the applied tensile load and the fibre displacement and is particularly suitable for synthetic fibres that may exhibit large axial elongation and slip-hardening interface behavior. Indeed, the balance conditions between the axial load and the shear stress arising on the fibre surface in frictional contact with the matrix are imposed on the deformed configuration. The frictional bond strength is assumed to increase with slippage distance as a consequence of the increasing abrasion of the fibre surface occurring for polymeric fibres that have been subjected to surface treatments. The model is also suitable for metallic fibres if constant friction or slip-softening interface behavior is assumed instead. The results provided by the proposed model are compared with the results obtained from pullout tests performed on polymeric fibres embedded in a cement matrix, both for treated and untreated fibres. After conveniently setting the constitutive parameters, the model proves to be able to predict the experimental curves accurately.

Peer-review under responsibility of the Gruppo Italiano Frattura (IGF).

Keywords: fracture toughness, ductility, fibre-reinforced concrete, pullout test, slip-hardening interface behavior

1. Introduction

In order to fix the peculiar disadvantages of the use of concrete in civil engineering applications, consisting in brittleness and low tensile strength, steel reinforcements are traditionally introduced in structural components in order to improve considerably the mechanical behavior of concrete. However, steel bar placing requires time and increases notably the production costs. Therefore, the practice of incorporating discrete fibres of various nature (e.g. glass, steel, plastic, carbon, kevlar) in the cement matrix at the mixing stage becomes very popular in the last decades, because it significantly enhances strength, fracture toughness and durability of the cast, hinders crack formation and growth and increases impact resistance [1]. The resulting mixture is known as Fibre Reinforced Concrete (FRC).

* Corresponding author. Tel.: +39 0522 522221 ; fax: +39 0522 522609.
E-mail address: enrico.radi@unimore.it

Peer-review under responsibility of the Gruppo Italiano Frattura (IGF).

In the past, only steel fibres were regarded as structural, providing diffuse reinforcement in agreement with the traditional steel bars. Later, the adoption of synthetic fibres increases due to some substantial advantages over metallic ones, such as strong chemical stability in alkaline and generally aggressive environments, convenient stocking and handling, a-toxicity and electromagnetic transparency. Moreover, the adoption of structural synthetic fibres lends a reliable reinforcement for shrinkage, operative stress and durability of the cast. Finally, polypropylene-based synthetic fibres significantly increase the fire resistance of the mixture by means of the so-called "spalling phenomenon". Due to these advantages over the metallic fibres, synthetic fibres have seen an increase of their commercial attractiveness in recent years. However, the main weakness in the use of synthetic fibres consists in the poor interfacial bond strength. Therefore, the improvement of the adhesion characteristics becomes necessary in order to take full advantage of the mechanical properties of FRC. A recent study [2] showed that the deposition of silica nanoparticles directly on the surface of synthetic fibres through a sol-gel treatment may significantly increase the bond strength and consequently improve the ductile properties of FRC structural components. The interfacial bond enhancement was investigated by performing pullout tests on single fibre from a cement matrix and then comparing the maximum load and the pullout energy absorbed for treated and untreated fibres. The test results showed that the load-displacement curve increase remarkably its magnitude for treated fibres, especially after the complete debonding of the fibre, namely when the largest bond strength is involved. As long as the tensile strength of the fibre is not exceeded, the observed slip-hardening interface behavior is a very desirable property in FRC, since it is generally accompanied by large energy absorption capacity.

The aim of the present study is to understand the mechanical behavior of FRC members by developing a simple but accurate analytical model for the pullout process, which is suitable for different kinds of fibres. As reported from different authors [3,4], the matrix deformation and the Poissons effect can be neglected in fibre pullout analysis, so that a one-dimensional model may result as adequate to describe the process. In order to simulate the response of pullout test accurately, it becomes however essential to take into account for the frictional behavior between fibre and matrix properly. The phenomenological model developed here takes into consideration arbitrarily large elongation of the fibre by imposing the balance conditions on the deformed configuration and, thus, it is particularly adapt for synthetic fibres, which may exhibit significant elongation. In particular, the contribution of frictional stress has been calculated on the deformed fibre surface and the deformation of the cement matrix has been neglected with respect to the fibre elongation. As the load is applied, the fibre is first bonded to the matrix along its embedded length and an almost linear elastic relation between the applied load and the fibre displacement is observed from the tests [2]. Then, as the load is increased the fibre start debonding from the loaded fibre end and the load-displacement curve becomes strongly non-linear. Depending on the fibre material and the kind of surface treatment performed on it, different kinds of interface bonding relationship can be modelled. Generally, the bond strength increases with the slippage distance for synthetic fibres as a consequence of the increase in the interface friction stress due to the abrasion of the fibre surface and accumulation of wear debris during the pullout process. For this kind of fibres, a large tensile load is usually required to pull the fibre out of the matrix also after the complete fibre debonding, up to the complete fibre extraction. On the contrary, a drastic reduction of the bond strength is observed during the pullout of steel fibres as a result of the breakdown of the cement at the fibre-matrix interface [3].

The experimental results obtained by Di Maida et al. [2] have been deprived from the viscous deformation calculated according to the simple *Maxwell* model, before comparing them with the prediction of the analytical model here proposed. However, the present model neglects the viscous deformation of the embedded part of the fibre, although this aspect may become important for synthetic fibres. A fibre pullout model considering also the viscous behavior will be proposed in a forthcoming paper.

2. Governing equations

The proposed model assumes elastic behavior of the fibre and a non-linear interface relationship between the shear stress τ and the slippage distance s between the fibre and the surrounding matrix. Since the matrix is assumed as rigid then $s(x)$ coincides with the displacement of the fibre section placed at abscissa x in the undeformed configuration. The elastic deformation experienced by the matrix has been taken into account by assuming an initial elastic response of the interface, up to the limit value $\bar{s}$ of the slippage distance s. When $s > \bar{s}$ then debonding occurs between fibre

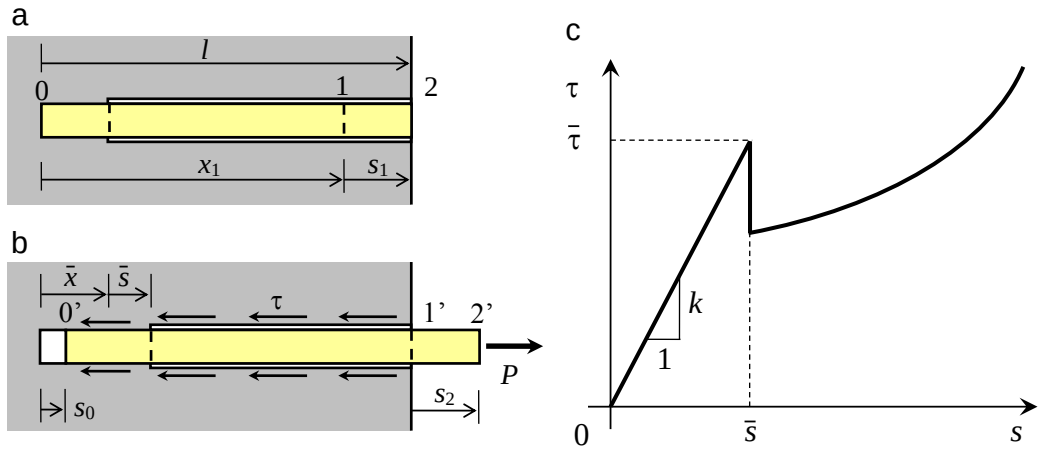

Fig. 1: (a) undeformed configuration with elastically bonded and frictionally debonded regions; (b) corresponding deformed configuration; (c) interface constitutive model between shear stress and slippage distance.

and matrix and frictional sliding takes place along the interface. The frictional bond strength is assumed to vary with the slippage distance according to an assigned interface relationship.

Let us consider a fibre embedded in a matrix for a length l and subject to the tensile load P. Let $\bar{x}$ denotes the section of the fibre placed between the elastic and frictional response of the interface in the undeformed configuration (Fig. 1a), such that $s(\bar{x}) = \bar{s}$. Moreover, let x_1 denotes the position in the undeformed configuration of the fibre section actually on the outer surface of the specimen, as illustrated in Fig. 1b. Correspondingly, three distinct regimes can be observed during the pullout test. At first, an *elastic stage* occurs when the fibre is bonded to the matrix along its full length. In this case, the interface behaves elastically at every point and the relation between τ and s may be assumed as linear. Then, a *debonding stage* originates when the fibre starts debonding from the matrix from the outer region towards the inner part. This kind of behavior is experienced if the displacement $s(x)$ is larger than the limit value $\bar{s}$, namely for $\bar{x} \le x \le x_1$, whereas for $0 \le x \le \bar{x}$ the interface behaves elastically. Finally, when the debonded region extends to the full embedded fibre length, then a *pullout stage* takes place. It starts when the displacement of the initial section of the fibre $s(0)$ becomes larger than the limit elastic value $\bar{s}$ and it finishes with the complete pullout of the fibre, namely when $s(0)$ reaches the embedded fibre length l.

The shear stress $\tau(s)$ along the embedded fibre length is assumed to vary according to the following piecewise discontinuous law

$$\tau(s) = \begin{cases} ks & \text{for} \quad s \le \bar{s} \quad (\text{i.e. for} \quad 0 \le x \le \bar{x}) \\ \tau_0 + as + bs^2 & \text{for} \quad s > \bar{s} \quad (\text{i.e. for} \quad \bar{x} < x \le x_1). \end{cases} \tag{1}$$

The constitutive model assumed for the interface behavior is depicted in Fig. 1c. Wang et al. [3] assumed a similar trend for the frictional bond strength, but they neglected the initial linear response exhibited when the fibre is elastically bonded to the matrix, since it has a limited influence on the pullout behavior displayed after complete debonding of the fibre. Namely, they assumed $\bar{s} = 0$. In this case, no slippage occurs along the bonded surface of the fibre and consequently no shear stress arises therein. According to the present model instead, the shear stress in the elastically bonded region attains a maximum at $x = \bar{x}$ and it decays as x tends to 0.

The axial strain ε of the fibre at the generic abscissa x in the reference (undeformed) configuration is given by

$$\varepsilon(x) = \frac{\pi d}{EA} \int_0^x \tau(t)(1 + \varepsilon(t))dt, \qquad \text{for} \quad 0 \le x \le x_1, \tag{2}$$

where no axial load is supposed to act on the initial section at $x = 0$ and $A = \pi d^2/4$ is the area of the cross section of diameter d. Note that the axial strain is given by $\varepsilon(x) = s'(x)$ where the prime denotes derivation with respect to x. The study is now split into the three stages occurring in succession during the pullout test.

2.1. Elastic stage

The initial elastic stage occurs for $s_1 \le \bar{s}$, where $s_1 = s(x_1)$. The displacement $s(x)$ in the elastically bonded region of the fibre, namely for $0 \le x \le \bar{x}$, is provided by the following ODE obtained by taking the derivative of eqn (2) and using eqn (1)

$$s'' = 2\gamma(1 + s')s, \tag{3}$$

where $\gamma = 2k/(dE)$. Then, by integrating eqn (3) and imposing the boundary condition $\varepsilon(0) = 0$, one obtains

$$\varepsilon - \log(1 + \varepsilon) = \gamma(s^2 - s_0^2), \tag{4}$$

where $s_0 = s(0)$ denotes the unknown displacement of the initial section at $x = 0$. Eqn (4) can be solved for ε by introducing the Lambert function [5], defined as $W_{-1}(x) := \left\{y \in (-\infty, -1] \,:\, ye^y = x,\ \forall x \in [-e^{-1}, 0)\right\}$, namely

$$\varepsilon = -1 - W_{-1}(-e^{-1-\gamma(s^2-s_0^2)}). \tag{5}$$

By integrating (5) between 0 and x, remembering that $\varepsilon(x) = s'(x)$, one finds

$$x = -\int_{s_0}^{s(x)} \frac{ds}{1 + W_{-1}(-e^{-1-\gamma(s^2-s_0^2)})}. \tag{6}$$

In particular, for $x = \bar{x}$ eqn (6) writes

$$\bar{x} = -\int_{s_0}^{\bar{s}} \frac{ds}{1 + W_{-1}(-e^{-1-\gamma(s^2-s_0^2)})}, \tag{7}$$

being $\bar{s} = s(\bar{x})$. For $x = \bar{x}$, eqn (4) provides

$$\bar{\varepsilon} - \log(1 + \bar{\varepsilon}) = \gamma(\bar{s}^2 - s_0^2), \tag{8}$$

where $\bar{\varepsilon} = \varepsilon(\bar{x})$. The latter equation can be solved for s_0, namely

$$s_0 = \sqrt{\bar{s}^2 - \gamma^{-1}[\bar{\varepsilon} - \log(1 + \bar{\varepsilon})]}, \tag{9}$$

where γ has been defined after eqn (3). The displacement $s_1 = l - x_1$ of section at $x = x_1$ then follows from (6) as

$$s_1 = l + \int_{s_0}^{s_1} \frac{ds}{1 + W_{-1}(-e^{-1-\gamma(s^2-s_0^2)})}. \tag{10}$$

Eqn (5), for $x = x_1$, gives

$$\varepsilon_1 = -1 - W_{-1}(-e^{-1-\gamma(s_1^2-s_0^2)}), \tag{11}$$

where $\varepsilon_1 = \varepsilon(x_1)$. Note that eqn (10) provides an implicit relation between s_0 and s_1. By using this relation, then eqn (11) yields ε_1 as a function of s_1.

2.2. Debonding stage

As the load increases, a stable debonding process occurs along the interface starting from the loaded fibre end. An elastically bonded region is present in the inner part of the fibre during the debonding stage since $s_0 \le \bar{s}$. The axial strain $\varepsilon(x)$ and the displacement $s(x)$ of the section in the debonded region, namely for $\bar{x} \le x \le x_1$ are related by eqn (2). As observed in Sec. 2.1, by taking the derivative of eqn (2) one has

$$s'' = \frac{4}{dE}(1 + s')\tau(s). \tag{12}$$

Integration of eqn (12) for $\bar{x} < x \le x_1$ with the imposition of the boundary condition at $x = \bar{x}$, namely $\varepsilon(\bar{x}) = \bar{\varepsilon}$, and using eqn (8), which holds at the boundary between bonded and debonded regions, then yields

$$\varepsilon - \log(1+\varepsilon) = T(s) - T(\bar{s}) + \gamma(\bar{s}^2 - s_0^2) \tag{13}$$

where

$$T(s) = \frac{4}{dE}\int \tau(s)\, ds = \kappa s + \alpha s^2 + \beta s^3, \qquad \kappa = \frac{4\tau_0}{dE}, \qquad \alpha = \frac{2\,a}{dE}, \qquad \beta = \frac{4\,b}{3\,dE}, \tag{14}$$

according to the constitutive relation (1). By introducing the Lambert function, eqn (13) can be solved for ε

$$\varepsilon = -1 - W_{-1}(-e^{-1-T(s)+T(\bar{s})-\gamma(\bar{s}^2-s_0^2)}). \tag{15}$$

Integration of eqn (15) from $\bar{x}$ to arbitrary x gives

$$x = \bar{x} - \int_{\bar{s}}^{s(x)} \frac{ds}{1 + W_{-1}(-e^{-1-T(s)+T(\bar{s})-\gamma(\bar{s}^2-s_0^2)}))}. \tag{16}$$

If eqn (16) is written at $x = x_1$ then the axial displacement of the section at $x = x_1$, namely $s_1 = l - x_1$, follows as

$$s_1 = l - \bar{x} + \int_{\bar{s}}^{s_1} \frac{ds}{1 + W_{-1}(-e^{-1-T(s)+T(\bar{s})-\gamma(\bar{s}^2-s_0^2)})}, \tag{17}$$

where $\bar{x}$ is given by eqn (7) as a function of s_0 only. By imposing the condition $\varepsilon(x_1) = \varepsilon_1$ on eqn (13) evaluated at $x = x_1$, it follow that

$$\varepsilon_1 - \log(1+\varepsilon_1) = T(s_1) - T(\bar{s}) + \gamma(\bar{s}^2 - s_0^2). \tag{18}$$

The latter equation can be solved for s_0, thus providing

$$s_0 = \sqrt{\bar{s}^2 - \gamma^{-1}\left[\varepsilon_1 - \log(1+\varepsilon_1) - T(s_1) + T(\bar{s})\right]}. \tag{19}$$

The introduction of eqn (19) for s_0 and eqn (7) for $\bar{x}$ in eqn (17) then provides an implicit relation between ε_1 and s_1, which holds during the debonding stage.

2.3. Pullout stage

The pullout stage starts after the complete debonding of the fibre, namely when $\bar{x} = 0$. During this stage the displacement s of a generic section of the fibre is larger than the limit elastic slippage $\bar{s}$. Then eqn (12) holds for $0 \le x \le x_1$. After the integration of eqn (12) and the imposition of the boundary conditions at $x = 0$, namely $\varepsilon(0) = 0$, it follows

$$\varepsilon - \log(1+\varepsilon) = T(s) - T(s_0), \tag{20}$$

where the function $T(s)$ has been introduced in eqn (14). Integration of eqn (20) for x between 0 and x_1 then provides the following relation between $s_1 = l - x_1$, and s_0

$$s_1 = l + \int_{s_0}^{s_1} \frac{ds}{1 + W_{-1}(-e^{-1+T(s_0)-T(s)})}. \tag{21}$$

Eqn (20) can be solved for ε and then evaluated at $x = x_1$

$$\varepsilon_1 = -1 - W_{-1}(-e^{-1-T(s_1)+T(s_0)}). \tag{22}$$

Finally, the elimination of the parameter s_0 from eqn (21) and eqn (22) provides the relation between ε_1 and s_1 during the pullout stage.

Since the displacement of the section 2 placed on the outer surface of the specimen in the undeformed configuration is given by $s_2 = s_1(1+\varepsilon_1)$, then the relation between ε_1 and s_2 follows straightly once the relation between ε_1 and s_1 has been found for each of the three stages. In particular, the theoretical pullout curves have been obtained by considering increasing values of the displacement s_1 from 0 up to the embedded fibre length l and obtaining the corresponding value of ε_1 from the trascendental equations which hold during each stage.

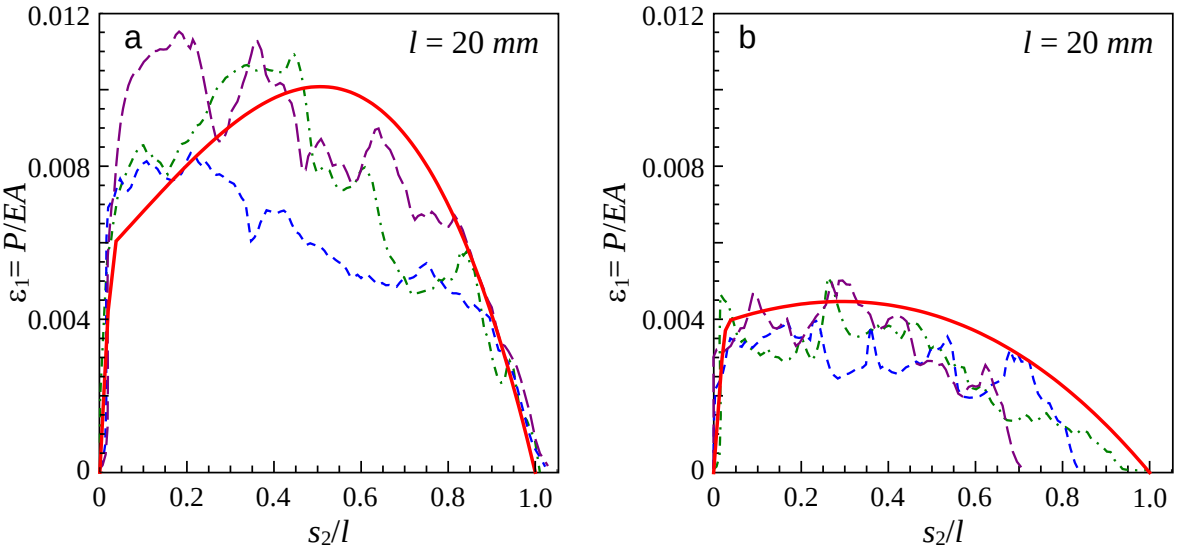

Fig. 2: Variation of axial strain $\varepsilon_1 = P/EA$ versus s_2/l: comparison between the theoretical curve (continuous line) and three experimental curves (dashed line) for (a) treated and (b) untreated fibres with embedded length $l = 20$ mm.

3. Viscous deformation

For synthetic fibres it becomes necessary to account for the viscous displacement of the fibre. Indeed, at the end of the pullout process, the fibre does not recover instantaneously his original length but it exhibits a residual displacement due to viscous behavior of the material. With reference to the *Maxwell* model, the elongation rate of the outer part of the fibre at the generic instant t is given by the sum of both elastic and viscous contributions, namely

$$\dot{u} = \dot{u}_e + \dot{u}_v = \frac{L\,\dot{P}(t)}{EA} + \frac{P(t)}{c} \tag{23}$$

where L is the length of the outer part of the fibre, E the elastic modulus, and c the dumping coefficient. Integrating $\dot{u}_v$ from eqn (23), being $s = Vt$, where V is the constant displacement rate imposed by the actuator, one finds

$$u_v(t) = \frac{1}{c}\int_0^t P(t)dt = \frac{1}{cV}\int_0^s P(s)ds. \tag{24}$$

Since at the end of the test the elastic displacement u_e must vanish together with the applied load, then the coefficient c can be found also from the residual viscous displacement as

$$u_{v,res} = s_{2,f} - l = \frac{1}{cV}\int_0^{s_{2,f}} P(s)ds \tag{25}$$

where $s_{2,f}$ is the displacement of the section 2 at the end of the pullout tests and the integral in eqn (25) is the area under the load-displacement curve obtained from the pullout test. The analytical results provided by the present model are compared in Figs. 2, 3 with the results of three pullout tests on polypropylene fibres treated by sol-gel technique [2]. The experimental results have been previously deprived of the contribution from elastic and viscous deformation of the outer part of the fibre.

4. Results and conclusions

The theoretical results provided by the model here developed have been compared with experimental results obtained from pullout tests on macro synthetic fibres embedded in a cement matrix [2].

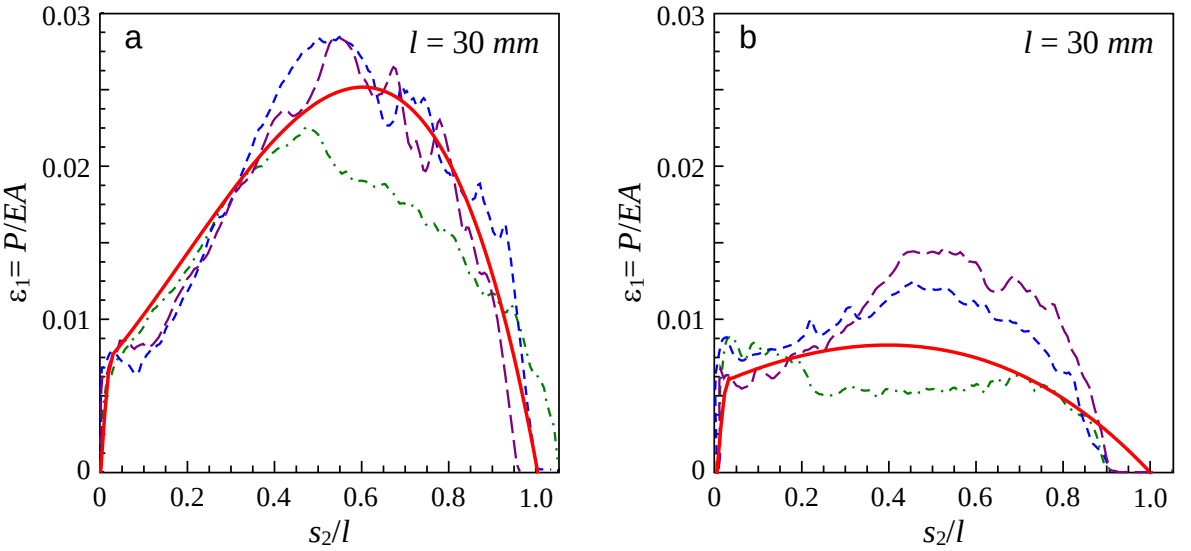

Fig. 3: Variation of axial strain $\varepsilon_1 = P/EA$ versus s_2/l: comparison between the theoretical curve (continuous line) and three experimental curves (dashed line) for (a) treated and (b) untreated fibres with embedded length $l = 30\,\text{mm}$.

The elastic behavior of the interface is defined by two constitutive parameters, namely the elastic stiffness of the interface $k = EA/l$ and the limit slippage distance $\bar{s}$. The elastic modulus has been determined by tensile tests performed on the synthetic fibres as $E = 6\,\text{GPa}$, whereas the limit slippage distance $\bar{s}$ has been extrapolated from the results of the pullout test as $\bar{s} = 0.5\,\text{mm}$. According to eqn (1), the debonding response of the interface is defined by three constitutive parameters, namely τ_0, a and b, which define the frictional bond strength of the interface as a quadratic function of the slippage distance. These three parameters have been determined empirically such that the theoretical curves turn out to be reasonably close to the test results. In particular, the following values have been assumed for untreated fibres $\tau_0 = 0.231\,\text{N/mm}^2$, $a = 0.0241\,\text{N/mm}^3$ and $b = 0.000\,243\,\text{N/mm}^4$, whereas for treated fibres these parameters significantly increased to $\tau_0 = 0.337\,\text{N/mm}^2$, $a = 0.0538\,\text{N/mm}^3$ and $b = 0.003\,37\,\text{N/mm}^4$. The theoretical and experimental load-displacement curves for treated and untreated fibres are plotted in Figs. 2, 3, respectively. Two different embedded fibre lengths have been considered, namely $l = 20\,\text{mm}$ and $l = 30\,\text{mm}$. As observed in [2] from the test results, the ratio between the load required to pullout treated and untreated fibres is about two. In terms of pullout energy the ratio increases to three. These significant differences are a consequence of the improvement in the bond strength of treated fibres, which yields an increase in the abrasion phenomena occurring at the outer surface of the fibre during the pullout test. Indeed, the higher is the rate of abrasion the higher is the peak of the pullout curve and the larger is the area under the curve.

Since the displacement measured during the pullout test encloses the contributions from the elastic and viscous elongation of the outer part of the fibre of length $L = 110\,\text{mm}$ [2], placed between the cement matrix and the testing machine grip, then these contributions have been removed from the experimental data before comparing them with the theoretical predictions, according to the results of Section 3.

The contribution of viscous deformation is more appreciable for treated fibres then for untreated ones, since the tensile load for treated fibres is much higher. Moreover, a significant load is required up to the complete extraction of the treated fibre, whereas for untreated fibres the tensile load tends to vanish before the fibre has been completely extracted, due to the loss of bonding properties.

From the curves plotted in Figs. 2, 3 it can be observed that the theoretical model closely predicts the experimental results, both for treated and untreated fibres, especially during the pullout stage. In particular, the model is able to capture the significant increase in the tensile load observed for the longer embedded fibre length (Figs. 3a, 3b).

The analytical results have been obtained by assuming a continuous relations between shear stress τ and slippage distance s, namely no loss of shear stress between elastically bonded and debonded region has been considered,

although it could be simulated by the present theoretical model. Indeed, the theoretical predictions turn out to be influenced by the slip-hardening parameters τ_0, a and b, which describe the frictional bond strength at debonding and pullout stages, much more than by the parameters defining the elastic behavior in the bonded region.

The present results prove that the adopted interface constitutive model is almost independent of the geometry and loading conditions. However, the constitutive parameters τ_0, a and b are mainly related to the adhesion properties between fibre and matrix. Therefore, they strongly depend on the surface treatment performed on the fibre and their definition may require a further investigation of the adhesion mechanisms based on a micromechanical approach.

With additional considerations on fibre orientation and distribution, the model here developed can be used also for predicting the equivalent flexural strength ratio $R_{e,3}$ for FRC [6], according to the material of the fibres and the surface treatment performed on them. The latter parameter is fundamental for the evaluation of the collapse load of FRC structural elements, such as beams and plates [7–9].

In conclusions, the present work proposes an accurate one-dimensional analytical model for simulating the pullout process of synthetic fibres from a cement matrix, which is able to take into consideration the improvement in the adhesion characteristics behavior exhibited by treated fibres. Although in the present study the model has been set and compared, for his validation, with pullout tests performed on synthetic fibres treated with nano-silica, it can be adopted also for different kinds of fibres and surface treatments by properly setting the constitutive parameters. Since the pullout test can simulate the fibre bridging phenomenon during the fracture process of FRC, the present model can be also conveniently employed in the study of the fracture process in this kind of innovative materials with enhanced ductile properties.

Acknowledgements

Financial support from “Fondazione Cassa di Risparmio di Modena” within the project “Bando di Ricerca Applicata 2013/2014 - fibra di carbonio e resina IPN” (convention C15414 protocol nr. 182.14.8C) is gratefully acknowledged.

References

[1] L. Lanzoni, A. Nobili, A.M. Tarantino, Performance evaluation of a polypropylene-based draw-wired fibre for concrete structures, Constr. Build. Mat. 28 (2012) 798-806.
[2] P. Di Maida, E. Radi, C. Sciancalepore, F. Bondioli, Pullout behavior of polypropylene macro-synthetic fibres treated with nano-silica, Constr. Build. Mat. 82 (2015) 39-44.
[3] Y. Wang, V.C. Li, S. Backer, Modelling of fibre pull-out from a cement matrix. Int. J. Cem. Compos. Lightweight Concr. 10 (1988) 143-149.
[4] Z. Lin, V.C. Li, Crack bridging in fiber reinforced cementitious composites with slip-hardening interfaces. J. Mech. Phys. Solids. 45 (1997) 763-787.
[5] R. M. Corless, G. H. Gonnet, D. E. G. Hare, D. J. Jeffrey, D. E. Knuth, On the Lambert W function, Adv. Comput. Math. 5 (1996) 329-359.
[6] The Concrete Society, Concrete industrial ground floors - a guide to design and construction, third ed., Technical Report No. 34, 2003.
[7] L. Lanzoni, E. Radi, A. Nobili, Ultimate Carrying Capacity of Elastic-Plastic Plates on a Pasternak Foundation, ASME J. Appl. Mech. 81 051013 (2014) 1-9.
[8] A. Nobili, E. Radi, L. Lanzoni, A cracked infinite Kirchhoff plate supported by a two-parameter elastic foundation, J. Eur. Ceramic Soc. 34 (2014) 2737-2744
[9] E. Radi, P. Di Maida, Analytical solution for ductile and FRC plates on elastic ground loaded on a small circular area, J. Mech. Mat. Struct. 9 (2014) 313-331